

Supplementary Materials

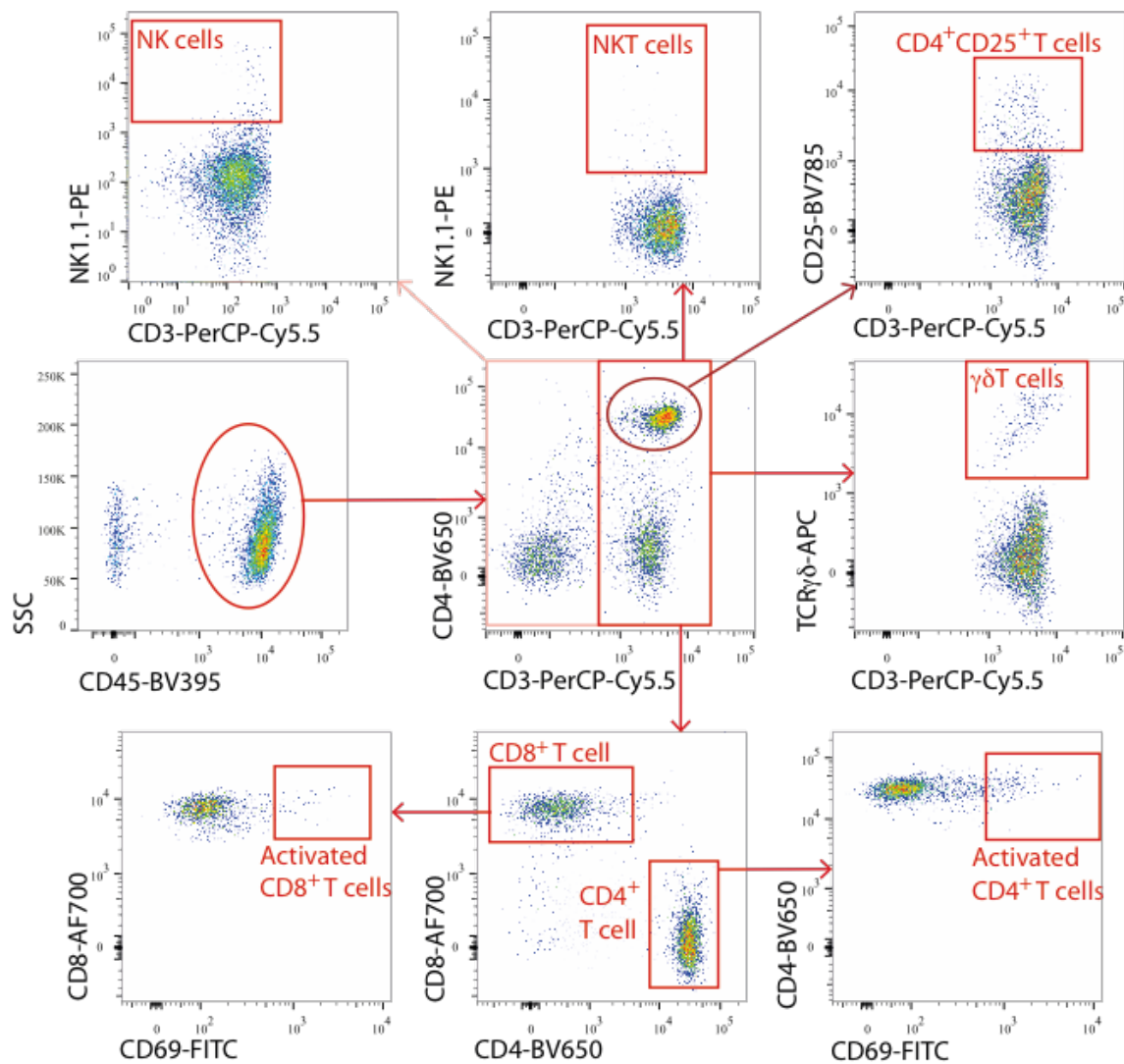


Figure S1. Gating strategy for identifying T cell subsets. Single cell suspensions prepared from draining LNs were surface stained with antibodies against T cell markers. Anti-CD45-BV395 was used to define the lymphocyte population. Anti-CD3e-PerCP-Cy5.5 was used to define the total T cells. T cells were then further subdivided into CD4⁺ T Cells, CD8⁺ T cells, NKT cells, $\gamma\delta$ T cells based on staining with anti-CD4-BV650, anti-CD8a-AF700, anti-NK1.1-PE and anti- $\gamma\delta$ TCR-APC respectively. T-regs were defined by gating on CD25-BV785⁺ cells from the double positive cells of the CD4-BV650 vs CD3e-PerCP-Cy5.5 scatter plot. NK cells were defined as CD3⁻ and NK1.1⁺ cells. CD69-FITC was used to measure the activation status of the T cell subsets.

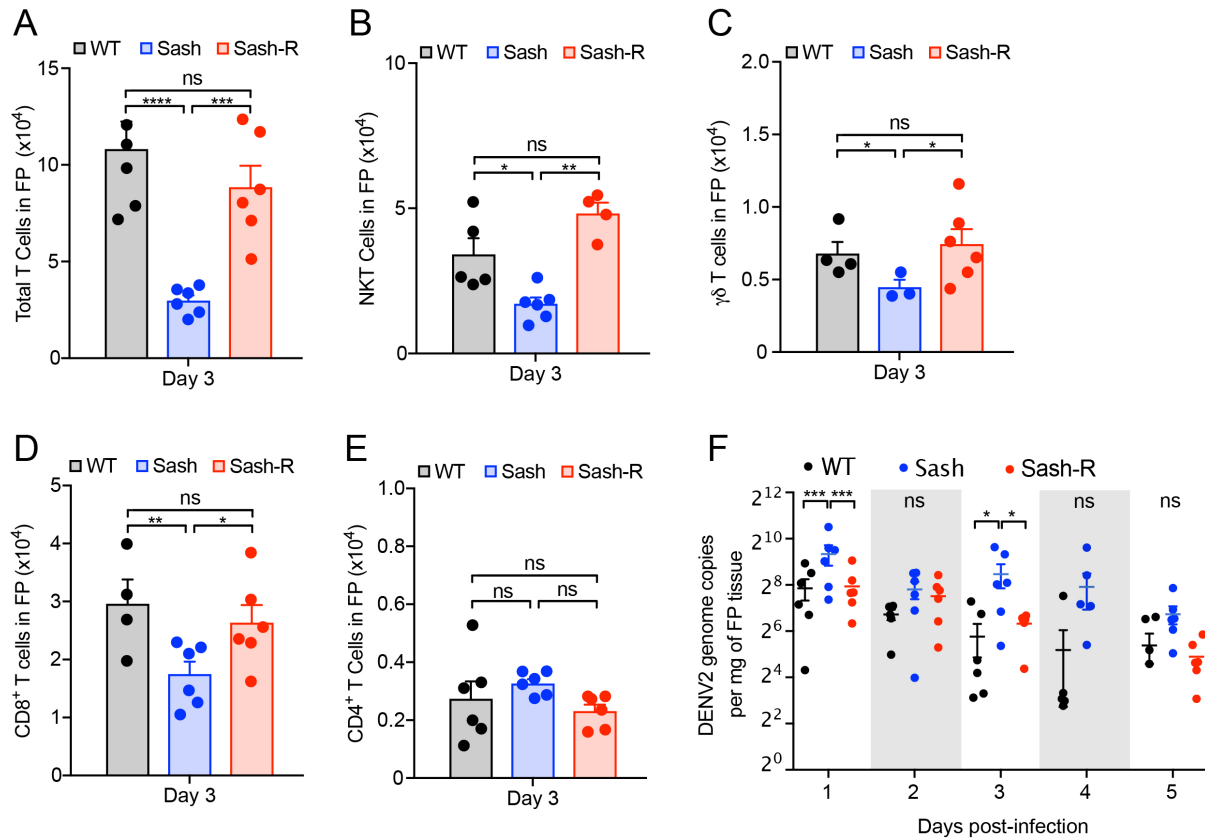


Figure S2. Reconstitution of MCs in Sash mice restores the T cell recruitment to the FP skin and enhances virus clearance. Sash mice reconstituted (Sash-R) with 1×10^7 BMMCs were infected with DENV2 by subcutaneous injection in FP skin. Tissues were harvested on day 3 post-infection and subpopulations of T cells were determined by staining the cells with antibodies against CD45, CD3, CD4, CD8, NK.1, and $\gamma\delta$ TCR. Comparisons of numbers of (A) Total T cells ($CD3^+$) (B) NKT cells ($CD3^+NK1.1^+$) (C) $\gamma\delta$ T cells ($CD3^+\gamma\delta TCR^+$) (D) CD8⁺ T Cells ($CD3^+CD8^+$) and (E) CD4⁺ T cells ($CD3^+CD4^+$) in WT, Sash and Sash-R mice indicate that MC reconstitution is sufficient to restore the recruitment of these cell types to the FP skin in Sash mice. (F) MC reconstitution enhanced the virus clearance from skin, since Sash-R had by lower genome copy numbers of DENV2 in FP skin compared to Sash mice. Data represent mean \pm SEM; and * $p < 0.05$, ** $p < 0.01$, *** $p < 0.001$, determined by 1-way (for panels A-E) or two-way (for panel F) ANOVAs, with Holm-Sidak's multiple comparisons test to obtain p-values, $n=4-6$ mice per group.

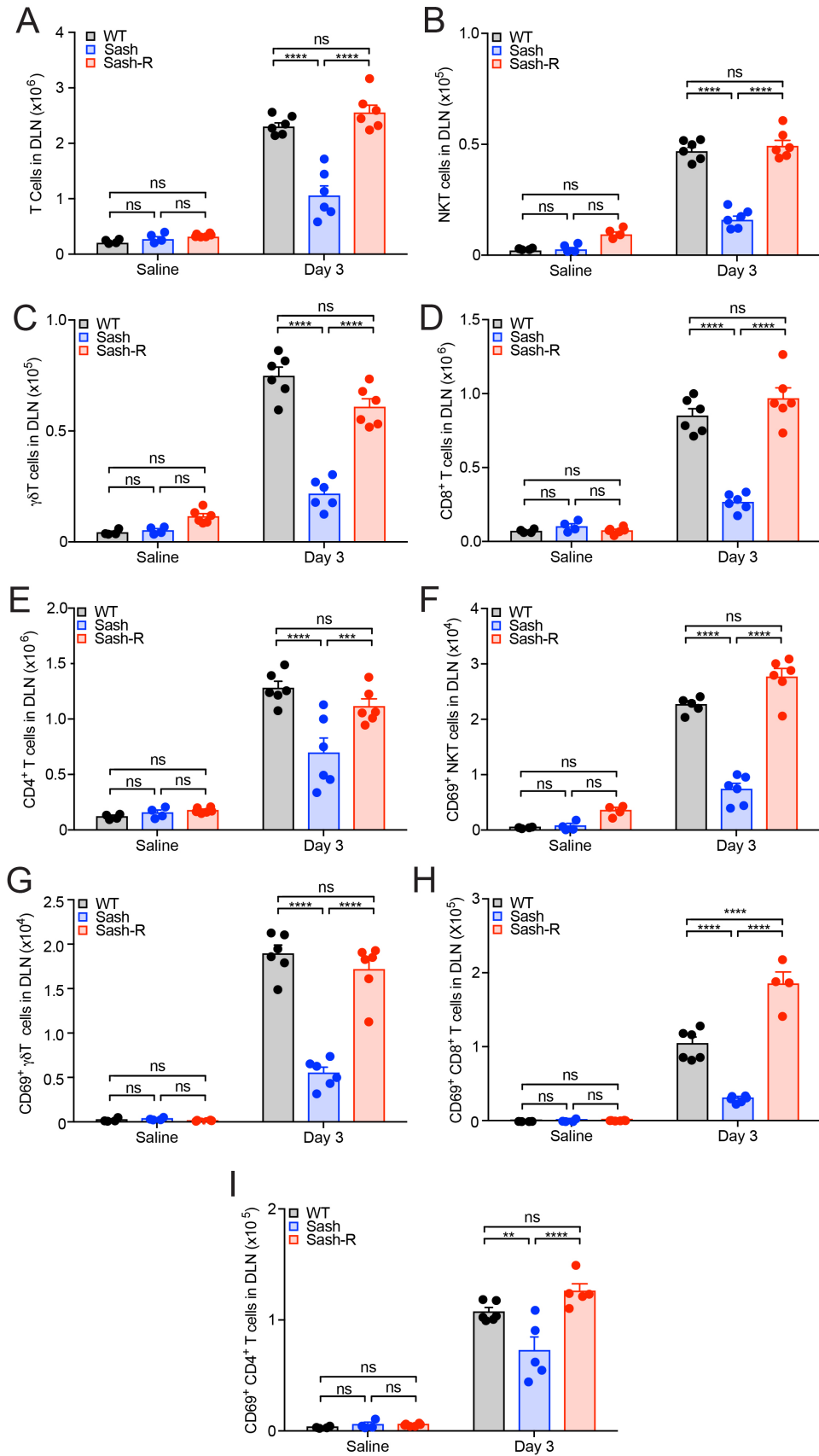


Figure S3. Reconstitution of MCs in Sash mice restores the T cell recruitment to the LN. Comparisons of numbers of (A) Total T cells ($CD3^+$) (B) NKT cells ($CD3^+NK1.1^+$) (C) $\gamma\delta$ T cells ($CD3^+\gamma\delta TCR^+$) (D) CD8⁺ T Cells ($CD3^+CD8^+$) and (E) CD4⁺ T cells ($CD3^+CD4^+$) in

WT, Sash and Sash-R mice indicate that MC reconstitution is sufficient to restore the recruitment of these cell types to the LNs. Numbers of activated (**F**) NKT, (**G**) $\gamma\delta$ (**H**) CD8 and (**I**) CD4 cells, by CD69 expression, were also restored in Sash-R mice. Data represent mean \pm SEM; and * $p < 0.05$, ** $p < 0.01$, *** $p < 0.001$, determined by 1-way ANOVA, with Holm-Sidak's multiple comparisons test to obtain p-values, n=4-6 mice per group.

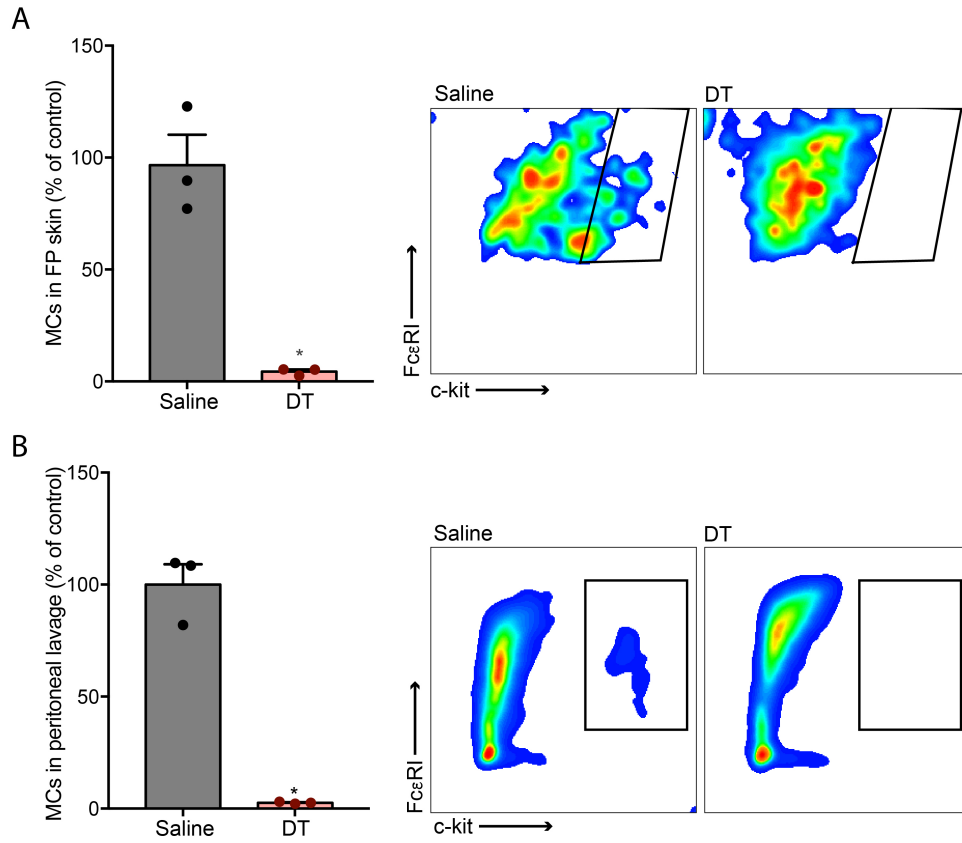


Figure S4. Efficient depletion of MCs after DT injection in MCPT5-cre iDTR model. *Mcpt5-cre/iDTR* mice ($n=3$) were injected with saline or DT as described in Figure 3a and were euthanized one week after the last injection for collection of FP skin and peritoneal lavage. Peritoneal cells were then stained with antibodies against CD45, FcεR1α and c-kit. **(A)** FP skin showed ~95% depletion of MCs. **(B)** Peritoneal MCs showed ~97% depletion. Data represent mean \pm SEM; * $p<0.05$ (by Student's unpaired t-test, 2-tailed). Representative flow cytometry plots demonstrating depletion are provided for Saline-injected and DT-injected groups in both panels **A-B**.

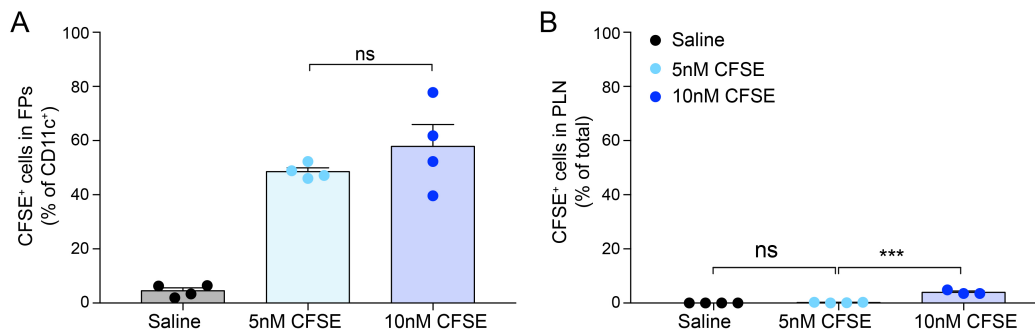


Figure S5. Efficiency of CFSE labeling in FP skin and draining LNs. FP skin were injected with multiple concentrations of CFSE and the efficiency of CFSE labelling of skin-resident DCs was measured 4h after injection. 5nM CFSE was selected for further experiments as (A) increasing the concentration did not lead to any significant increase in labelling of DCs and (B) increased slightly the CFSE⁺ cell numbers in DLN. After 5nM CFSE injection, no CFSE⁺ cells could be detected in the peripheral LN (PLN). Data represent mean \pm SEM, *** $p < 0.001$ by 1-way ANOVA, $n = 3-4$ mice per group.

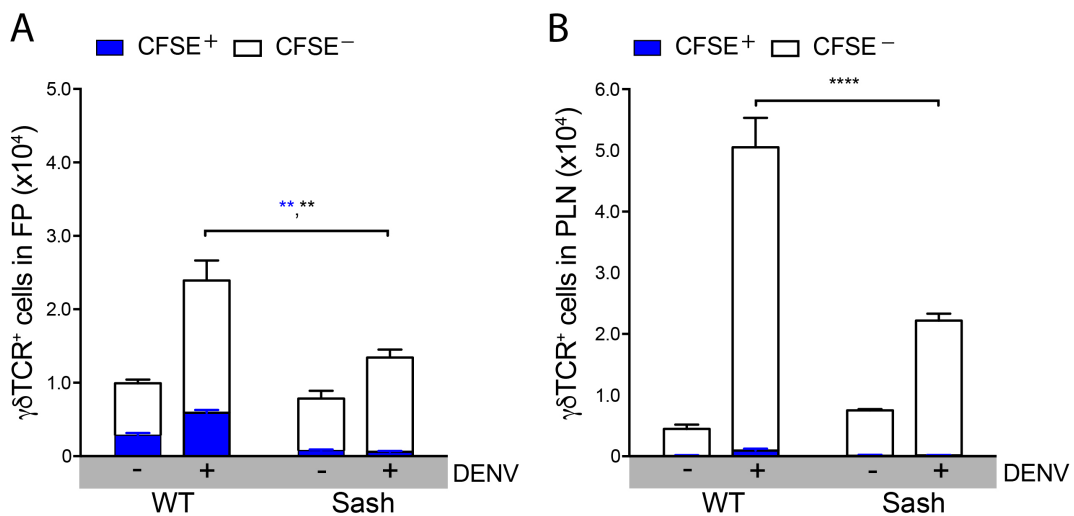


Figure S6. Increase in $\gamma\delta$ T cells in DENV-infected LNs is due to both recruitment and proliferation. WT and Sash mice were injected with CFSE, 4h prior to infection by subcutaneous footpad injection with 1×10^5 pfu of DENV. FPs and DLNs were collected 72h post-infection and $\gamma\delta$ T cells ($CD3^+ \gamma\delta TCR^+$) were analyzed by flow cytometry. (A) WT mice showed an increase in numbers of CFSE⁺ cells (in blue) as well as CFSE⁻ newly-recruited $\gamma\delta$ T cells in response to infection, while in Sash mice the slight increase in total $\gamma\delta$ T cell numbers is due to recruitment of CFSE⁻ $\gamma\delta$ T cells to the LN. (B) CFSE⁺ $\gamma\delta$ T cells migrated from the footpad to the draining LNs only in WT mice and significantly higher numbers of CFSE⁻ $\gamma\delta$ T cells were also retained in the draining LNs of WT mice in response to DENV infection, compared to the Sash mice. Data represent mean \pm SEM, ** $p < 0.01$, **** $p < 0.0001$ (by two-way ANOVA with Sidak's multiple comparison test) and $n = 4-6$ mice per group.

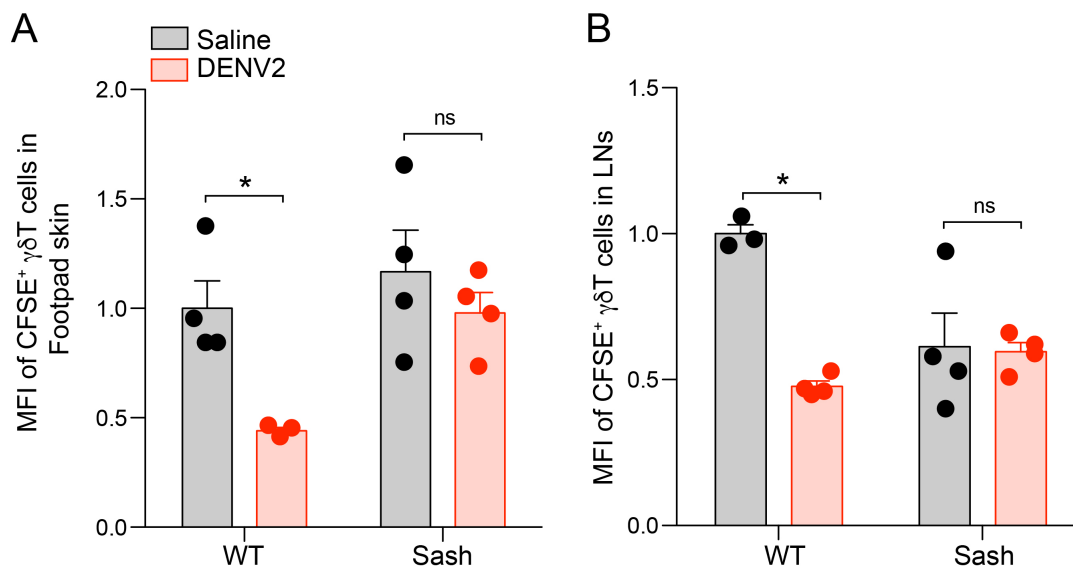


Figure S7. CFSE dilution supports $\gamma\delta$ T cell proliferation in vivo. WT and Sash mice were injected with CFSE, 4h prior to subcutaneous injection in FPs with either 1×10^5 pfu of DENV or saline. Median CFSE fluorescence intensity (MFI) of $\gamma\delta$ T cells from **(A)** FPs and **(B)** draining LNs 24h post-infection showed significant decreases in the fluorescence intensity only in WT mice, indicating these cells underwent proliferation. Data represent mean \pm SEM, * $p < 0.05$ by two-way ANOVA with Tukey's multiple comparison test $n=4$ mice per group.

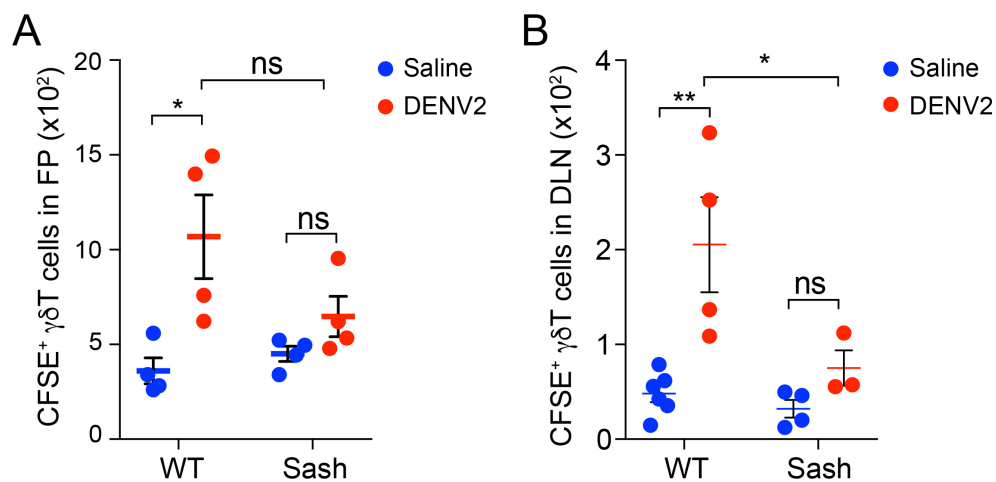


Figure S8. Recruitment of CFSE-labelled T cells to FPs and draining LNs. WT and Sash mice were injected with CFSE labelled splenocytes, 24h prior to subcutaneous injection in FPs with either 1×10^5 pfu of DENV or saline. Cells from FP skin and popliteal LNs were stained with anti-CD3 and anti- $\gamma\delta$ TCR, after harvesting 24h post-infection. Higher numbers of labelled $\gamma\delta$ T cells were detected both in **(A)** FPs and **(B)** draining LNs. Data represent mean \pm SEM; * $p < 0.05$, ** $p < 0.01$ by two-way ANOVA with Tukey's multiple comparison test, $n=4-6$ mice per group.

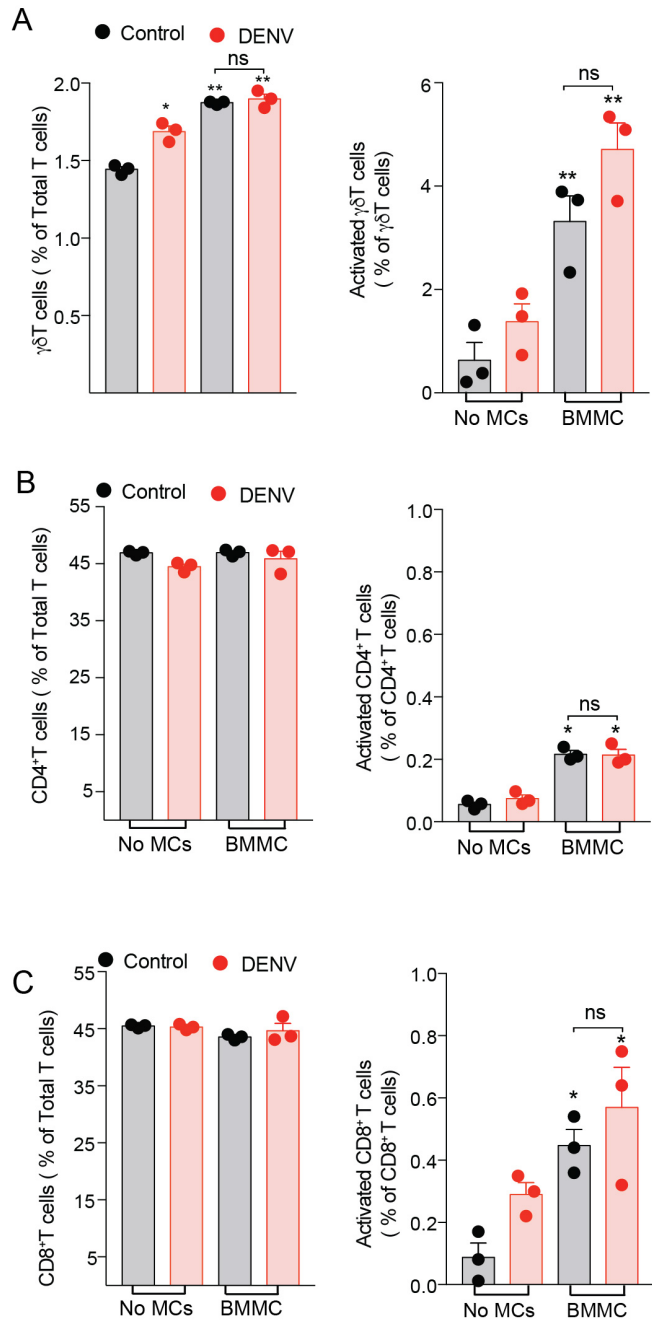


Figure S9. MCs induce proliferation and activation of $\gamma\delta$ T cells in co-culture. T cells isolated from naive mice (n=3) were cultured with BMMC in presence or absence of DENV to assess MC-dependent and DENV-dependent activation and proliferation of T cells. Cells were stained for CD3, CD4, CD8, CD69 and $\gamma\delta$ TCR and analyzed by flow cytometry after 48h of co-culture. The percentages of total and activated (A) $\gamma\delta$ (B) CD4⁺ and (C) CD8⁺ T cells were compared by 1-way ANOVA and considered significant for p<0.05. Data represent mean \pm SEM.

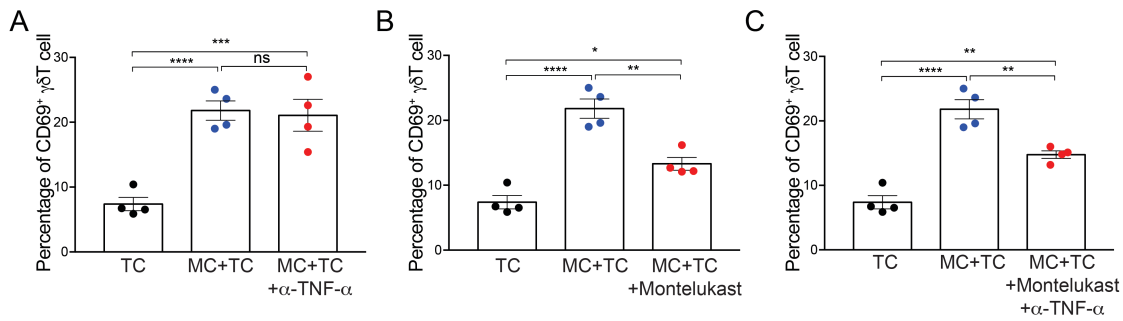


Figure S10. Baseline activation of $\gamma\delta$ T cells is enhanced by leukotrienes. BMMCs were co-cultured with T cells isolated from naïve mice ($n=4$) in the presence or absence of (A) TNF- α blocking antibody (0.5 μ g/mL) or (B) the leukotriene antagonist montelukast (10 μ M) or (C) both. Activation of $\gamma\delta$ T cells was measured 72h post co-culture by staining the cells with antibodies against CD3, $\gamma\delta$ TCR, CD69. Montelukast significantly inhibited the activation of $\gamma\delta$ T cells that is mediated by unstimulated MCs. Data represent mean \pm SEM; * $p < 0.05$, ** $p < 0.01$, **** $p < 0.0001$, by two-way ANOVA with Tukey's multiple comparisons test.

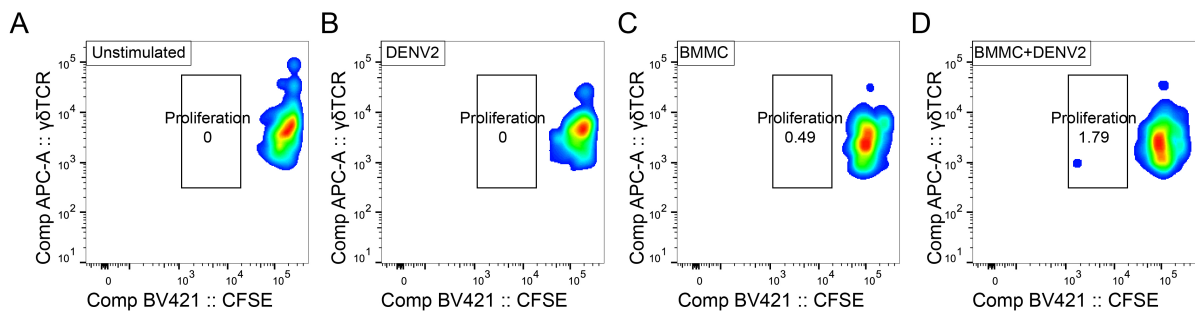


Figure S11. MCs promote $\gamma\delta$ T cell proliferation in co-culture. This figure contains representative plots ($n=3$) corresponding to Figure 5i. $\gamma\delta$ T cells isolated from naïve mice were labelled with CFSE and then were co-cultured with BMMC (1:1) in the presence or absence of DENV2 (1 MOI). After co-culture for 96h, cells were stained for flow cytometry. Proliferation of $\gamma\delta$ T cells (CD3⁺ $\gamma\delta$ TCR⁺) was measured by dilution of CFSE. Representative plot showing proliferation of $\gamma\delta$ T cells in groups that were (A) unstimulated (B) stimulated with DENV (C) co-cultured with BMMC or (D) co-cultured with DENV-challenged BMMCs.

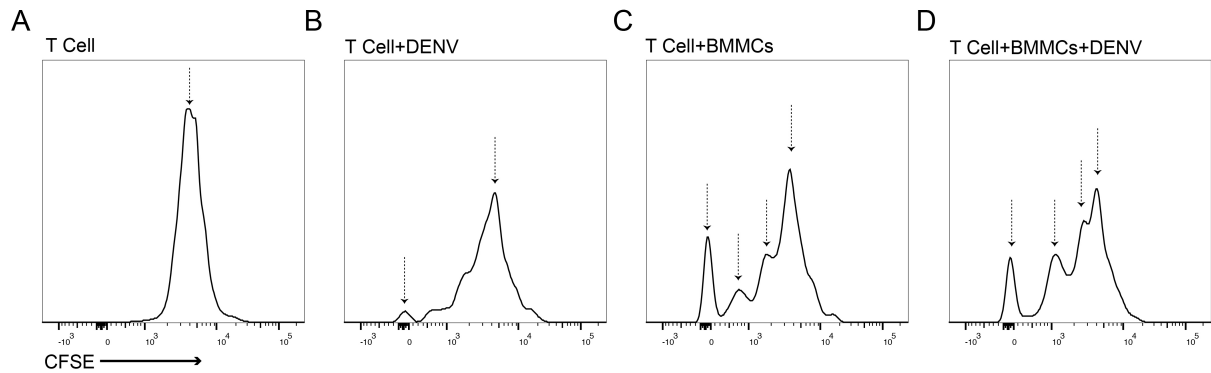


Figure S12. Step-wise dilution of CFSE supports T cell proliferation. T cells isolated from naive mice (n=3) were labelled with CellTrace CFSE and cultured with BMMC in presence or absence of DENV for 96h. Cells were stained with LIVE/DEAD™ Fixable Near-IR stain prior to staining with anti-CD3 and anti- $\gamma\delta$ TCR antibodies and analyzed by flow cytometry. Live $\gamma\delta$ T cells were analyzed for CFSE content. Representative histograms showing CFSE staining intensity in $\gamma\delta$ T cells in groups that were (A) unstimulated (B) stimulated with DENV (C) co-cultured with BMMC or (D) co-cultured with DENV-challenged BMMCs supports MC and DENV-specific proliferation of $\gamma\delta$ T cells.

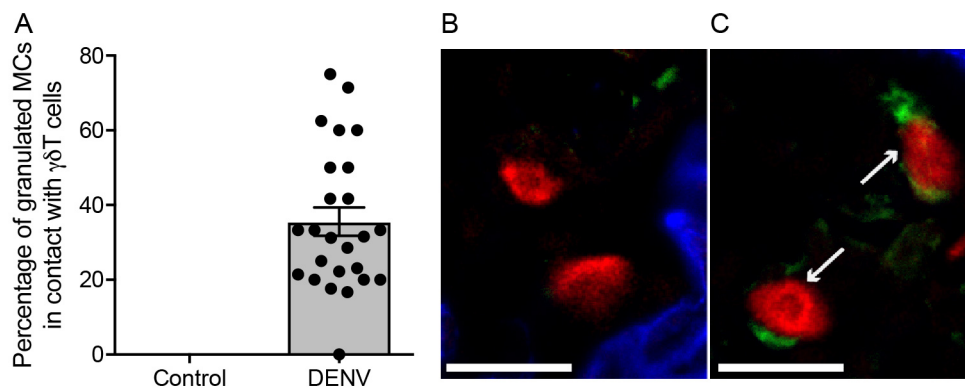
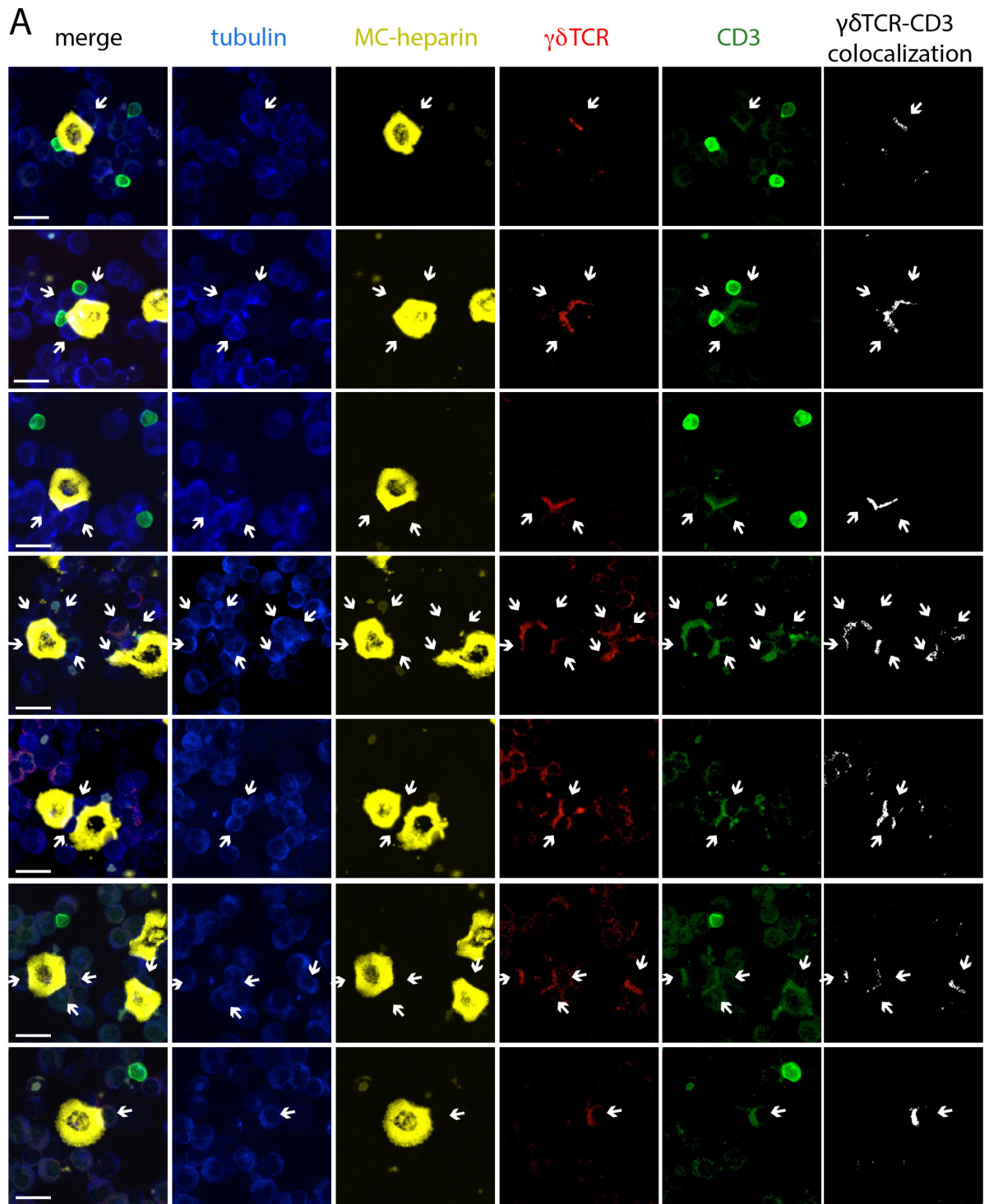


Figure S13. MCs form numerous contacts with $\gamma\delta$ T cells in vivo during DENV infection. FPs collected from WT mice injected with saline or 1×10^5 PFU of DENV2 were sectioned and stained for blood vessels (CD31, blue), $\gamma\delta$ TCR (green) and MC heparin (indicating MC granules, red). (A) Graph indicates the percentage of granulated MCs in contact with $\gamma\delta$ T cells in saline-injected control skin (not detected) and DENV-infected skin, 24h post infection. Data represent mean \pm SEM. (B-C) Representative confocal images of DENV-infected skin showing MCs (red) that are assessed as (B) not interacting with $\gamma\delta$ T cells (green) and (C) representative of MC- $\gamma\delta$ T cell interaction. For confocal images, CD31 staining of blood vessels appears blue. Scale bars For B-C, scale bar=20 μ m. Arrows point to MCs that are contacting $\gamma\delta$ T cells.



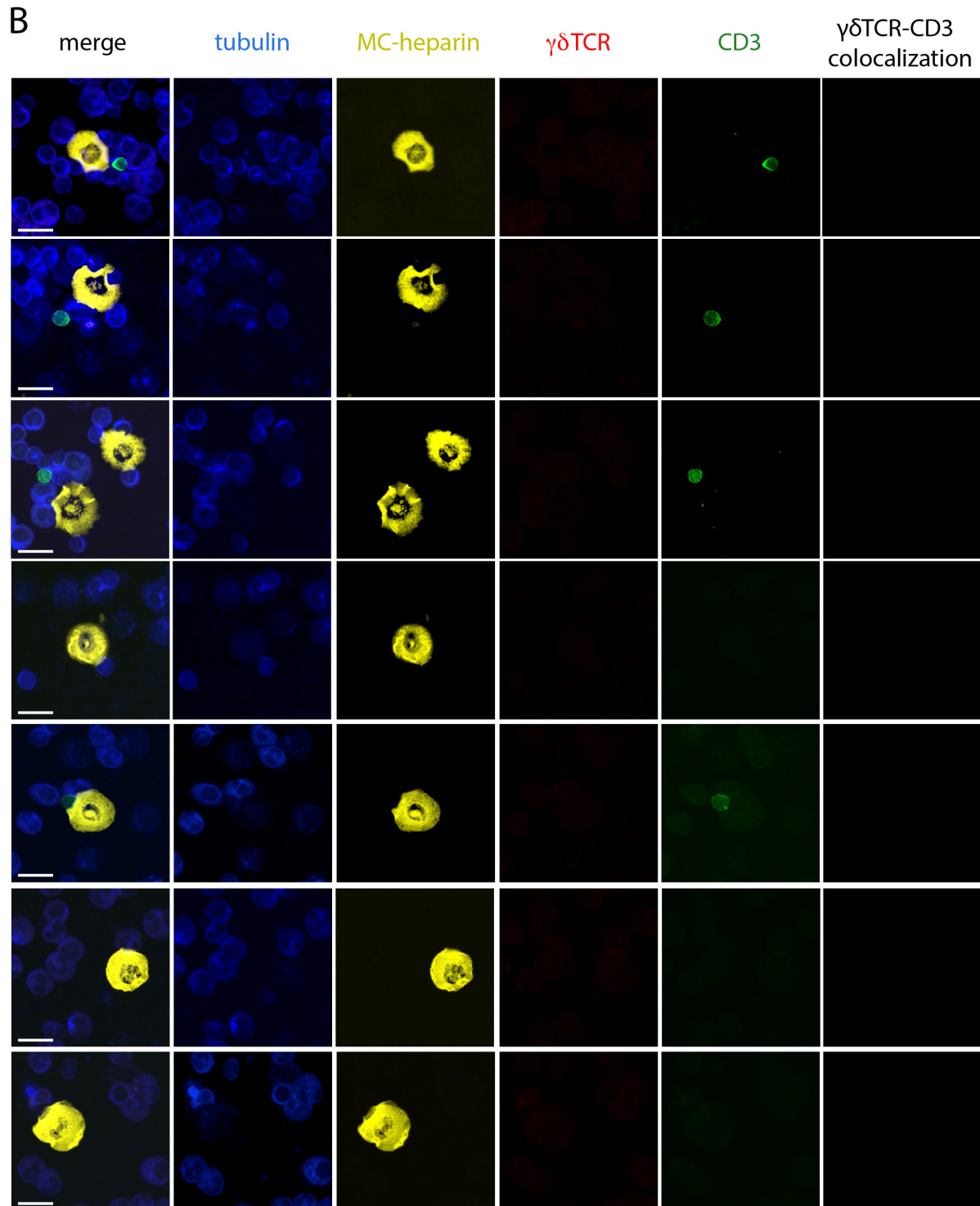


Figure S14. Additional images of peritoneal MC and $\gamma\delta$ T cell interactions during DENV infection and uninfected controls. Cells from peritoneal lavage samples collected 24h post injection with (A) DENV or (B) saline were cytospun onto slides and stained with an avidin-conjugated probe to highlight MC granules and antibodies against CD3, $\gamma\delta$ TCR and tubulin before visualisation by confocal microscopy. Scale bars=20 μ m. Arrows point to contact sites where polarized co-localization of CD3 and $\gamma\delta$ TCR occur.

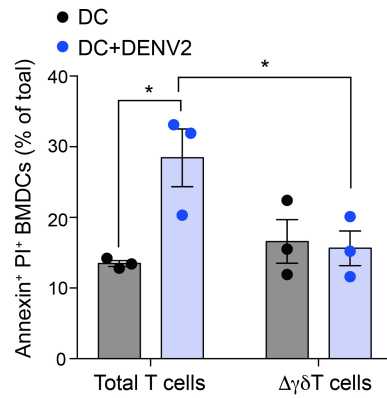


Figure S15. Death of $\gamma\delta$ T cell-exposed DENV-infected DCs occurs through apoptosis. Total T cells or T cells depleted of $\gamma\delta$ T cells ($\Delta\gamma\delta$ T cells) isolated from DENV-infected mouse LNs (n=3), 72hr post-infection, were co-cultured with BMDCs or BMDCs that were pre-infected 24h prior to co-culture with DENV (MOI 1). Cytotoxicity was measured after another 12h, by staining the cells with anti-CD11b-PE (eBiosciences), anti-CD11c-PacificBlue (Invitrogen), Annexin-V-FITC and propidium iodide (BD Biosciences). Data represent mean \pm SEM; *p < 0.05, by two-way ANOVA, with Tukey's multiple comparisons test to compute p-values.

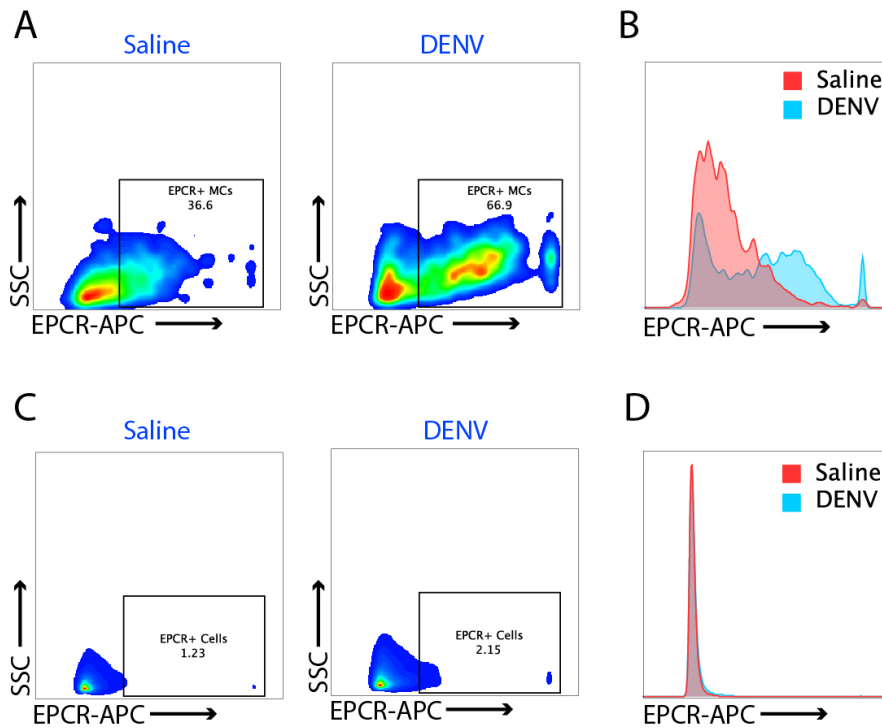


Figure S16. DENV induces EPCR expression by MCs in vivo. WT mice (n=6) were infected with DENV2 subcutaneously in FPs and cell surface expression of EPCR on LN MCs ($c\text{-kit}^+ \text{Fc}\epsilon\text{R1}\alpha^+$) was measured by flow cytometry after 24h. Representative flow cytometry plots show (A) increases in numbers of EPCR-expressing MCs and (B) increased expression of EPCR on MCs in the draining LNs of infected mice. Representative plots also indicate that no increase in (C) numbers of EPCR-expressing non-MCs or (D) levels of EPCR expression on the non-MCs in the LNs were observed.

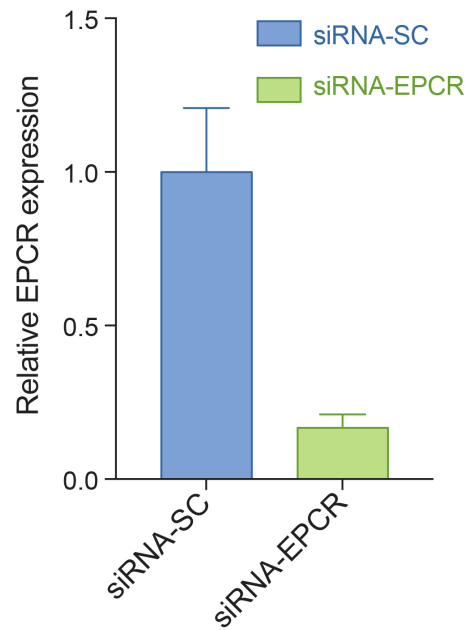


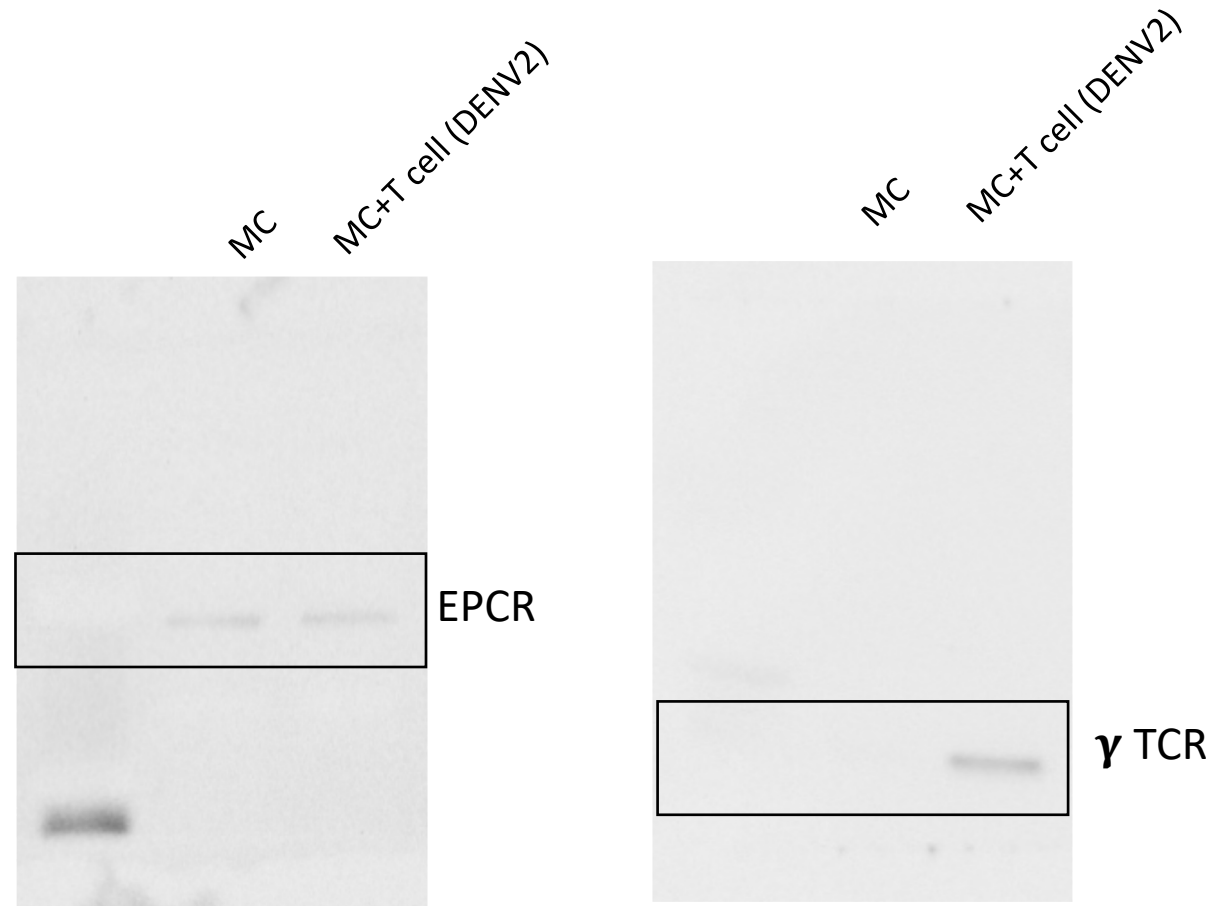
Figure S17. Efficient knock-down of EPCR expression by siRNA. A knock-down efficiency of ~86% was achieved 24h post-transfection of BMMCs with the si-RNA for EPCR compared to levels in BMMCs transfected by the scrambled control siRNA (siRNA-SC). Expression was measured by real-time PCR and the expression levels were normalised to GAPDH expression. Data represent mean \pm SEM and the experiment was done in triplicate.

Table S1: Primers

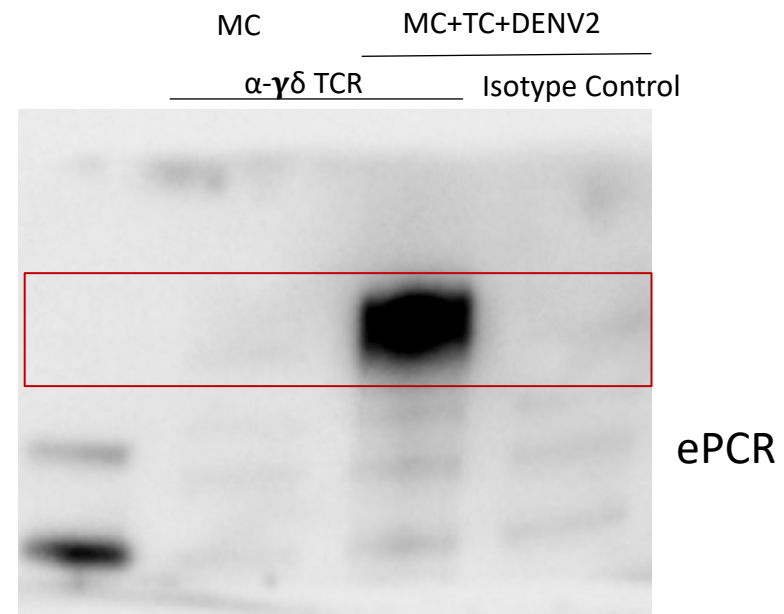
Virus Quantification	
DENV2	TTGCACCAACAGTCAATGTCTTCAGGTTTC
DENV2F	TCAATATGCTGAAACGCGCGAGAAACCG
DENV2R	CGCCACAAGGGCCATGAACAG
Chemokine expression analysis	
mCCL2F	GTTGGCTCAGCCAGATGCA
mCCL2R	AGCCTACTCATTGGGATCATCTTG
mCCL20F	GGAAGGAAGAGGCGTCTGTA
mCCL20R	ACTCCTGGAGCTGAGAATGG
mCCL25F	CCAAGGTGCCTTTGAAGACT
mCCL25R	TCCTCCAGCTGGTGGTTACT
mCCL27F	GGTTCTGGGGATGAACACAG
mCCL27R	ATAGACAGCCACTCCCAAGC
mCXCL10F	GACGGTCCGCTGCAACTG
mCXCL10R	GCTTCCCTATGGCCCTCATT
mActinF	GGGTGTGATGGTGGGTATGGGTCAG
mActinR	GCAGCACAGGGTGCTCCTCAGG
mGAPDH F	CGACTTCAACAGCAACTCCCACTCTTCC
mGAPDH R	TGGGTGGTCCAGGGTTTCTTACTCCTT

Panel 1 (Top)

Panel 2 (Bottom)



Panel 1 (Top)



Panel 2 (Bottom)

